Title

Ex Situ NMR Relaxometry of Metal–Organic Frameworks for Rapid Surface-Area Screening

Journal

Angewandte Chemie, 125(46)

ISSN

0044-8249

Authors

Chen, Joseph J
Kong, Xueqian
Sumida, Kenji
et al.

Publication Date

2013-11-11

DOI

10.1002/ange.201305247

Peer reviewed

NMR Porosity Screening of MOFs

DOI: 10.1002/anie.200((will be filled in by the editorial staff))

Ex-Situ NMR Relaxometry of Metal-Organic Frameworks for Rapid Surface Area Screening**

Joseph J. Chen, Xueqian Kong, Kenji Sumida, Mary Anne Manumpil, Jeffrey R. Long, and Jeffrey A. Reimer*

Metal-organic frameworks are porous crystalline solids consisting of metal clusters or ions connected via organic linkers. These frameworks can exhibit exceptional gas storage capacities and adsorptive selectivities;[1] these properties have led to their investigation for a vast number of applications.[2] However, optimization remains difficult due to the effectively infinite number of metal-ligand combinations and the large number of phases that can emerge for even a single choice of metal and ligand. Synthetic reaction conditions play a crucial role in determining which phase precipitates from solution. Thus, preparation of the desired material in pure, crystalline form relies on extensive systematic screening of many reaction parameters.[3] The modular nature of the solventothermal preparation of metal-organic frameworks makes high-throughput synthesis an effective means for rapidly exploring the parameter space.[4] However, the subsequent characterization of new compounds becomes a bottleneck for this type of workflow, since structural characterization by XRD or evaluation of the BET surface area via adsorption measurements are not practical for large numbers of unknown samples. Thus, the development of a porosity analysis tool that precludes the need to perform labor-intensive tasks (i.e. activation and sorption measurements) on each sample would greatly accelerate the discovery of potentially interesting frameworks by quickly eliminating non-porous or low-surface area materials that are not of interest.

Nuclear magnetic resonance (NMR) relaxometry can potentially provide an initial estimate of the pore volume and surface area of an unknown metal-organic framework. These methods use imbibed fluid nuclei as probes of the internal surface area and have been used extensively to characterize porous media, including rocks, silica, zeolites, cements, and soils.[5] Transverse relaxation (T_2) is a process in which observable magnetization decays to equilibrium in an exponential fashion.[6] The relaxation rate of liquid nuclei imbibed in porous media generally depends on the degree of confinement due to interactions with the pore walls[7] and internal field gradients.[8] Though some relaxation studies of hydrocarbon gases in MOF-5 and $Cu_3(BTC)_2$ have been conducted,[9] the relaxation behavior of liquids in metal-organic frameworks and its connection to internal surface area has yet to be studied systematically.

Herein, we demonstrate a correlation between the BET surface area and the transverse relaxation (T_2) of solvent-imbibed metal-organic frameworks and zeolites. The use of a liquid probe greatly simplifies sample preparation to washing and filtration, minimizing the amount of necessary automation hardware while eliminating the time-consuming process of sample isolation and activation. Furthermore, the relaxation measurements described in this study can be performed considerably faster than a typical BET surface area measurement. Lastly, the integration of autosampling hardware allows large numbers of samples to be screened without the need for manual sample transfer or instrument operation, providing a convenient initial screening method well-suited for integration into a high-throughput workflow (see Figure S8 in the SI). Note that this technique does not replace adsorption-based characterization experiments, but should facilitate the identification of a generally small fraction of highly porous materials within a combinatorial library of unknown samples, allowing researchers to perform time-consuming workup on the most promising frameworks.

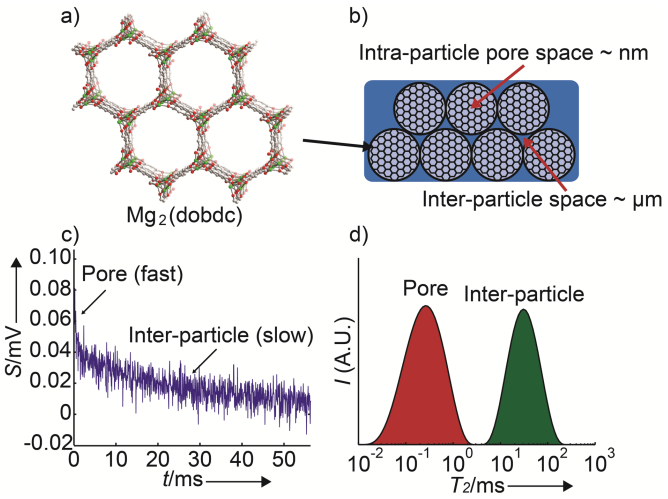

Figure 1. Illustration of the multiple-length scales that generate multi-exponential relaxation in $Mg_2(dobdc)$. (a) A portion of the crystal structure of $Mg_2(dobdc)$. Green, grey and red spheres represent Mg, C and O atoms, respectively, while H atoms are omitted for clarity; (b) length scales formed by packed porous particles; (c) NMR signal (S) vs. time (t) showing relaxation with slow and fast exponential decays; and (d) Laplace inversion of relaxation data with two relaxation populations corresponding to pore and inter-particle solvent.

Samples of solvent-imbibed metal-organic frameworks can be approximated as having two pore size regimes, as shown in Figure 1a and 1b using $Mg_2(dobdc)$ (Mg-MOF-74, CPO-27-Mg; $dobdc^{4-}$ = 2,5-dioxido-1,4-benzenedicarboxylate) as an example: nanometer-sized pores belonging to the inherent structure of the framework

[*] J. J. Chen, Dr. X. Kong, Dr. J. A. Reimer
Department of Chemical and Biomolecular Engineering
University of California, Berkeley, CA, 94703
E-mail: joseph.chen@berkeley.edu

Dr. K. Sumida, M. A. Manumpil, Dr. J. R. Long
Department of Chemistry
University of California, Berkeley, CA, 94703

[**] J. J. Chen and Dr. X. Kong contributed equally to this work. The information, data, or work presented herein was funded by the US Department of Energy, Advanced Research Projects Agency - Energy (ARPA-E) under Grant No. DE-AR0000103. The authors acknowledge Mr. J. A. Mason and Mr. A. Milner for assistance with the sample preparation and Fulbright New Zealand for partial support of K.S. The Laplace inversion software is used courtesy of Victoria University of Wellington.

Supporting information for this article is available on the WWW under http://www.angewandte.org or from the author.((Please delete if not appropriate))

(intra-particle) and micron-sized voids between the individual crystallites (inter-particle). Since solvent molecules are expected to diffuse slowly between the two types of pores, relaxation should exhibit multi-exponential behavior, where faster relaxation occurs for intra-particle solvent, and slower relaxation for inter-particle solvent (Figure 1c). An algorithm referred to as an inverse Laplace transform (ILT) or Laplace inversion, deconvolutes multi-exponential transverse relaxation into individual exponential components (Figure 1d).[10] As shown in Figure 2, the T_2 "relaxation spectra" of dimethyl sulfoxide (DMSO) protons imbibed in $Mg_2(dobdc)$[1] (Figure 1a; SA_{BET} = 1660 m^2g^{-1}) exhibits multi-exponential relaxation for a series of solvent contents. Note that DMSO was chosen as a probe solvent due to its common use in the synthesis of metal-organic frameworks and its inert nature towards most compounds. Relaxation measurements were conducted on samples with known amounts of solvent using single-sided NMR-MOUSE (**MO**bile **U**niversal **S**urface **E**xplorer). This setup measures the ^{1}H-NMR signal of samples placed outside the magnet,[11] simplifying the incorporation of automation hardware. T_2 relaxation was measured using a CPMG sequence[12] with an approximate experiment duration of 15-30 minutes.

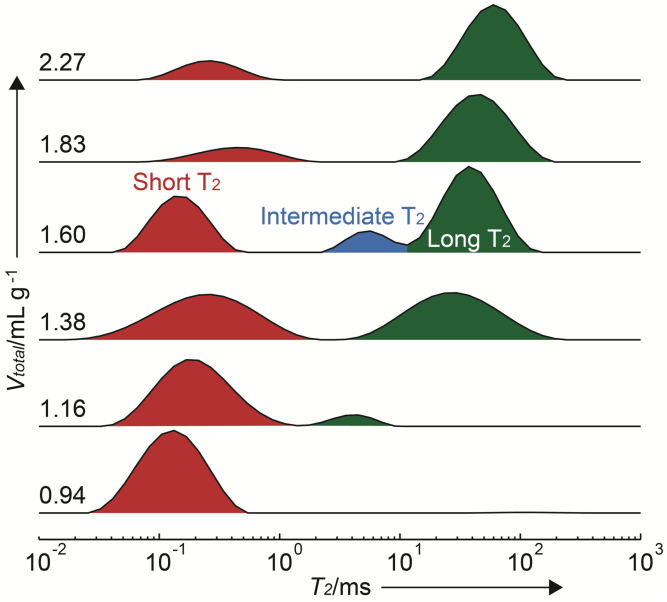

Figure 2. Profiles of T_2 relaxation times, or "relaxation spectra," for $Mg_2(dobdc)$ with various amounts of DMSO added (V_{total}). Solvent content is normalized to the mass of the evacuated framework. Relaxation times can be roughly grouped into short, intermediate, and long T_2 regimes. The total intensity at each solvent content is normalized to unity.

At low solvent content, a single peak appears, representing a population of solvent with a short T_2 (~10^{-2} to 10^0 ms). Due to the short relaxation times compared to neat DMSO ($T_{2,DMSO} \approx 300$ ms on the NMR-MOUSE), the protons associated with this relaxation population reside on solvent molecules confined within the one-dimensional channels of $Mg_2(dobdc)$. The presence of a single population indicates that little solvent exists in the inter-particle voids, which can be attributed to the much stronger solvent binding expected within the confines of the pores compared to the voids between the individual particles. As solvent is added, a second population appears at longer T_2 (10^0 to 10^3 ms), and the corresponding relaxation peak shifts to longer times. Since the pores are completely filled at higher solvent contents, this peak can be assigned to inter-particle solvent. Successive solvent addition leads to a greater proportion of molecules that interact weakly with the framework, causing the relaxation time to approach the value for neat DMSO. Notably, a third intermediate relaxation population occasionally appears with intermediate relaxation times (10^0 to 10^1 ms). This range of relaxation times also corresponds to that for the long-T_2 peaks at lower solvent content which suggests that the intermediate relaxation peaks correspond to solvent localized near the surface of the particles rather than inside the framework pores. Sufficiently fast diffusional exchange between the pores and inter-particle space during the NMR experiment would indeed generate an intermediate relaxation environment, as discussed later. Also, note that each relaxation population is represented by broad peaks spanning orders of magnitude, and given the low signal-to-noise ratio associated with using the NMR-MOUSE and the uniform pore size of metal-organic frameworks, the breadth of the spectrum represents an uncertainty originating from experimental noise rather than the existence of a wide pore size distribution.

Since the peak area in the relaxation spectrum is proportional to the number of spins (i.e., solvent volume) of that relaxation population, a connection between the pore volume and the relaxation behavior can be made. The surface area in microporous media is roughly proportional to the pore volume, and frameworks with high surface areas should exhibit relaxation spectra with proportionally larger short-T_2 peaks at a given solvent content. Indeed, the relaxation behavior for a variety of other samples, including low-surface area zeolites, metal-organic frameworks with paramagnetic metal centers (e.g., $Ni_2(dobdc)$[13]), or frameworks with higher dimensionality pores (e.g., UiO-66[14]), remains qualitatively similar to that for $Mg_2(dobdc)$ (see Supporting Information).

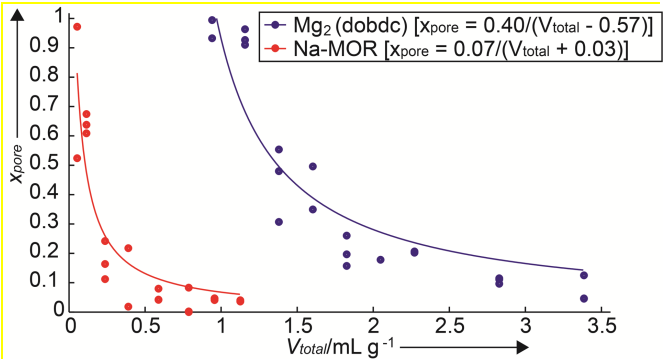

Figure 3. Decay of the fraction of total intensity (x_{pore}) encompassed by the pore-confined solvent plotted vs. increasing solvent content (V_{total}). The solid lines indicate the fits of the data with Eq. 1. Na-MOR is the zeolite sodium mordenite.

The fraction of total intensity encompassed by the short-T_2 peak corresponding to the solvent molecules within the micropores is shown in Figure 3 for $Mg_2(dobdc)$ and a low-surface area zeolite Na-mordenite (SA_{BET} = 398 m^2g^{-1}). Note that the short-T_2 peak is defined as the fastest relaxation population in "relaxation spectra" displaying multiple peaks. Spectra with single peaks are classified as belonging to either solvent within the pores or within the bulk liquid, depending on the magnitude of relaxation times. The fraction of

total signal associated with pores (x_{pore}) should be equal to the ratio of the normalized pore volume to the normalized total solvent content ($V_{pore}V_{total}^{-1}$). However, a small amount of strongly-bound immobile solvent may go undetected due to the extremely short relaxation times that these nuclei exhibit ($T_2 \sim 10$ µs). Therefore, the ratio for x_{pore} must be modified, resulting in the expression below.

$$x_{pore} = \frac{V_{pore} - V_{im}}{V_{total} - V_{im}} \quad (1)$$

V_{im} represents the normalized volume of immobile solvent, and the fits of Eq. 1 are shown in Figure 3. For Mg_2(dobdc), V_{im} is relatively large, while for Na-MOR, the V_{im} is small (and positive due to experimental noise), indicating that Mg_2(dobdc) binds solvent more strongly than Na-MOR, most likely due to the presence of open metal sites in Mg_2(dobdc). Figure 4 shows the correlation of V_{pore} with the experimental nitrogen BET surface area for a variety of porous materials imbibed with DMSO. *N*,*N*-Dimethylformamide (DMF), a ubiquitous solvent in metal-organic framework synthesis, was also used as a probe solvent with similar results. A satisfactory linear correlation can be applied (Figure 4), the results of which are shown in Table S1 in the SI.

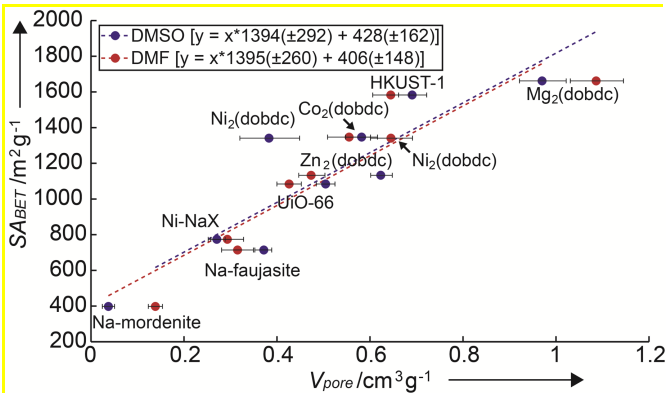

Figure 4. Correlation of BET surface area (SA_{BET}) to the fitted V_{pore} using DMSO and DMF. Dashed lines indicate the fit for each solvent. The error bars encapsulate the ILT error, the pore decay fitting error, and the error in NMR measurement. All samples were tested at RT.

The NMR-predicted surface area agrees well with the measured surface area, with error (± standard deviation) being dominated by the linear regression error that is expected to improve as more frameworks are tested and as the testing protocol is refined. The analysis clearly distinguishes low-porosity samples from high-surface area metal-organic frameworks, demonstrating its potential for implementation alongside high-throughput synthesis instruments. Also, the flexibility in solvent choice could further simplify sample preparation by enabling testing of as-synthesized frameworks.

A PDE model was developed to further elucidate the physics of a diffusing, heterogeneous framework-solvent system (see the SI for model details). This model (see Figure S20) utilizes the Bloch-Torrey equations to compute the evolution of NMR magnetization for a spherically-symmetric particle surrounded by varying amounts of bulk solvent. The inversion spectra derived from the analytical model qualitatively match the results found in actual experiments. Furthermore, this model supports the hypothesis that exchanging interfacial solvent produces intermediate relaxation peaks. Figure 5 compares the "relaxation spectra" of interfacial solvent with solvent away from the interface. The large intermediate peak in the spectra for interfacial solvent suggests that the interface is indeed an intermediate relaxation environment.

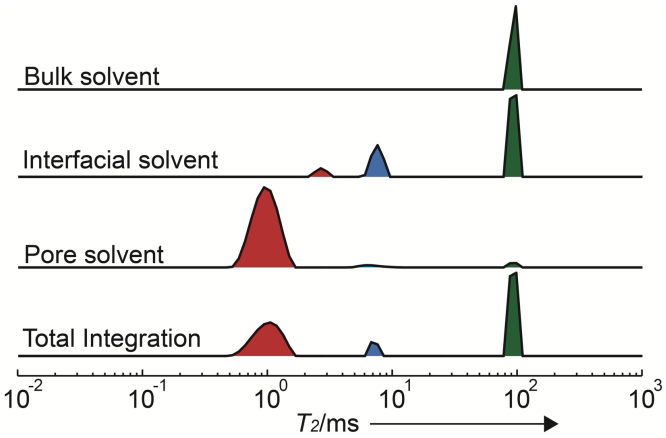

Figure 5. Laplace inversion of T_2 relaxation curves generated by the mathematical model based upon appropriate Bloch-Torrey equations. Inversions were performed on the separate relaxation signals from the pore solvent, the interfacial solvent, and the bulk solvent, as well as the total signal from all three. Further details on the model and the parameters used can be found in the SI.

The foregoing study has described a robust correlation relating the surface area of a wide variety of microporous media to the proton relaxation behavior of imbibed solvent, demonstrating the potential for NMR relaxometry as a high-throughput screening technique. The results were obtained on a portable NMR instrument that interfaces easily with combinatorial synthesis methods. Simulations using the Bloch-Torrey equations qualitatively confirm the observed behavior and allow the effects of solvent transport processes to be explored. Further optimization of sample preparation, measurement methodology, and NMR hardware should yield considerable reductions in error and measurement time (see SI). The inclusion of this technique in a high-throughput screening workflow is expected to expedite the discovery of new candidate materials for applications such as CO_2 capture.

Received: ((will be filled in by the editorial staff))
Published online on ((will be filled in by the editorial staff))

Keywords: high-throughput screening · metal-organic frameworks · microporous materials · NMR relaxometry · single-sided NMR

[1] a) S. R. Caskey, A. G. Wong-Foy, A. J. Matzger, *J. Am. Chem. Soc.* **2008**, *130*, 10870-10871; b) H. Furukawa, et al., *Science* **2010**, *329*, 424-428; c) J. A. Mason, K. Sumida, Z. R. Herm, R. Krishna, J. R. Long, *Energy Environ. Sci.* **2011**, *4*, 3030; d) T. M. McDonald, D. M. D'Alessandro, R. Krishna, J. R. Long, *Chemical Science* **2011**, *2*, 2022; e) A. R. Millward, O. M. Yaghi, *J. Am. Chem. Soc.* **2005**, *127*, 17998-17999; f) A. O. Yazaydın, A. I. Benin, S. A. Faheem, P. Jakubczak, J. J. Low, R. R. Willis, R. Q. Snurr, *Chem. Mater.* **2009**, *21*, 1425-1430; g) A. O. Yazaydın, et al., *J. Am. Chem. Soc.* **2009**, *131*, 18198-18199.

[2] a) J.-R. Li, Y. Ma, M. C. McCarthy, J. Sculley, J. Yu, H.-K. Jeong, P. B. Balbuena, H.-C. Zhou, *Coord. Chem. Rev.* **2011**, *255*, 1791-1823; b) K. Sumida, D. L. Rogow, J. A. Mason, T. M. McDonald, E. D. Bloch, Z. R. Herm, T. H. Bae, J. R. Long, *Chem. Rev.* **2012**, *112*, 724-781.

[3] a) S. S. Kaye, A. Dailly, O. M. Yaghi, J. R. Long, *J. Am. Chem. Soc.* **2007**, *129*, 14176-14177; b) N. Stock, S. Biswas, *Chem. Rev.* **2012**, *112*, 933-969; c) E. Biemmi, S. Christian, N. Stock, T. Bein, *Micropor. Mesopor. Mat.* **2009**, *117*, 111-117.

[4] a) R. Banerjee, A. Phan, B. Wang, C. Knobler, H. Furukawa, M. O'Keeffe, O. M. Yaghi, *Science* **2008**, *319*, 939-943; b) N. Stock, T. Bein, *Angew. Chem.* **2004**, *116*, 767-770; *Angew. Chem. Int. Edit.* **2004**, *43*, 749-752; c) K. Sumida, et al., *Chemical Science* **2010**, *1*, 184-191.

[5] a) R. Kleinberg, W. Kenyon, P. Mitra, *J. Magn. Reson.* **1994**, *108*, 206-214; b) P. J. Barrie, *Annu. Rep. NMR Spectrosc.* **2000**, *41*, 265-316; c) R. Brown, P. Fantazzini, *Phys. Rev. B* **1993**, *47*, 14823-14834; d) F. D'Orazio, S. Bhattacharja, W. Halperin, K. Eguchi, T. Mizusaki, *Phys. Rev. B* **1990**, *42*, 9810-9818; e) S. Davies, K. Packer, *J. Appl. Phys.* **1990**, *67*, 3163-3170; f) W. P. Halperin, J. Y. Jehng, Y. Q. Song, *Magn. Reson. Imaging* **1994**, *12*, 169-173; g) F. Jaeger, S. Bowe, H. Van As, G. E. Schaumann, *Eur. J. Soil. Sci.* **2009**, *60*, 1052-1064; h) J. Kärger, R. Valiullin, **2011**; i) W. Kenyon, J. Howard, A. Sezginer, C. Straley, A. Matteson, K. Horkowitz, R. Ehrlich, in *Trans. SPWLA Ann. Logging Symp., Vol. 30*, **1989**; j) J. P. Korb, *New J. Phys.* **2011**, *13*, 035016; k) P. McDonald, J. P. Korb, J. Mitchell, L. Monteilhet, *Phys. Rev. E* **2005**, *72*; l) J. Mitchell, J. D. Griffith, J. H. Collins, A. J. Sederman, L. F. Gladden, M. L. Johns, *J. Chem. Phys.* **2007**, *127*, 234701; m) L. Monteilhet, J. P. Korb, J. Mitchell, P. McDonald, *Phys. Rev. E* **2006**, *74*; n) H. A. Resing, *Adv. Mol. Relax. Int. Pr.* **1972**, *3*, 199-226; o) L. R. Stingaciu, L. Weihermüller, S. Haber-Pohlmeier, S. Stapf, H. Vereecken, A. Pohlmeier, *Water Resour. Res.* **2010**, *46*; p) R. Valckenborg, L. Pel, K. Kopinga, *J. Phys. D: Appl. Phys.* **2002**, *35*, 249; q) K. Washburn, P. Callaghan, *Phys. Rev. Lett.* **2006**, *97*.

[6] M. H. Levitt, *Spin dynamics*, Wiley Chichester, UK, **2001**.

[7] K. R. Brownstein, C. Tarr, *Phys. Rev. A* **1979**, *19*, 2446.

[8] a) M. D. Hürlimann, *J. Magn. Reson.* **1998**, *131*, 232-240; b) J. Mitchell, T. C. Chandrasekera, M. L. Johns, L. F. Gladden, *Phys. Rev. E* **2010**, *81*.

[9] a) D. I. Kolokolov, H. Jobic, A. G. Stepanov, J. Ollivier, S. Rives, G. Maurin, T. Devic, C. Serre, G. Férey, *J. Phys. Chem. C* **2012**, *116*, 15093-15098; b) T. Ueda, K. Kurokawa, Y. Kawamura, K. Miyakubo, T. Eguchi, *The Journal of Physical Chemistry C* **2012**, *116*, 1012-1019; c) M. Wehring, J. Gascon, D. Dubbeldam, F. Kapteijn, R. Snurr, F. Stallmach, *J. Phys. Chem. C* **2010**, *114*, 10527-10534.

[10] a) P. C. Hansen, *SIAM Rev.* **1992**, *34*, 561-580; b) J. Mitchell, T. C. Chandrasekera, L. F. Gladden, *Prog. Nucl. Magn. Reson. Spectrosc.* **2012**, *62*, 34-50; c) S. W. Provencher, *Comput. Phys. Commun.* **1982**, *27*, 213-227; d) L. Venkataramanan, Y. Q. Song, M. D. Hurlimann, *IEEE T. Signal Proces.* **2002**, *50*, 1017-1026.

[11] a) B. Blümich, J. Perlo, F. Casanova, *Prog. Nucl. Magn. Reson. Spectrosc.* **2008**, *52*, 197-269; b) G. Eidmann, R. Savelsberg, P. Blümler, B. Blümich, *J. Magn. Reson.* **1996**, *122*, 104-109; c) J. Perlo, F. Casanova, B. Blumich, *J. Magn. Reson.* **2005**, *176*, 64-70.

[12] a) H. Carr, E. Purcell, *Physical Review* **1954**, *94*, 630-638; b) S. Meiboom, D. Gill, *Rev. Sci. Instrum.* **1958**, *29*, 688-691.

[13] P. D. Dietzel, B. Panella, M. Hirscher, R. Blom, H. Fjellvag, *Chem. Commun.* **2006**, 959-961.

[14] J. H. Cavka, S. Jakobsen, U. Olsbye, N. Guillou, C. Lamberti, S. Bordiga, K. P. Lillerud, *J. Am. Chem. Soc.* **2008**, *130*, 13850-13851.

Relaxometry of MOFs

Joseph J. Chen,* Dr. Xuequian Kong, Dr. Kenji Sumida, Mary Anne Manumpil, Dr. Jeffrey R. Long, Dr. Jeffrey A. Reimer

Ex-Situ Relaxometry of Metal-Organic Frameworks for Rapid Surface Area Screening

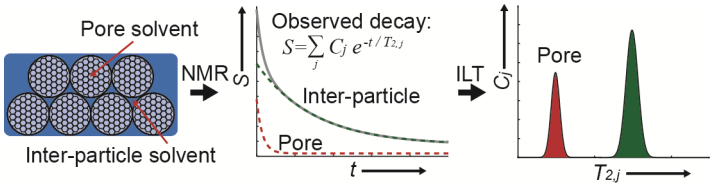

A robust characterization technique has been developed to estimate the surface area of a variety of microporous metal-organic frameworks and zeolites using the NMR relaxation behavior of imbibed solvent. This technique is amenable to automation and can expedite the characterization of microporous materials by identifying and discarding any non-porous or low-surface area structures precluding the need for time-consuming gas adsorption analysis.

Ex-Situ NMR Relaxometry of Metal-Organic Frameworks for Rapid Surface Area Screening**

Joseph J. Chen, Xueqian Kong, Kenji Sumida, Mary Anne Manumpil, Jeffrey R. Long, and Jeffrey A. Reimer*

*To whom all correspondence should be addressed. Phone: (510) 643-3073
E-mail: joseph.chen@berkeley.edu

Table of Contents

I. Sample Synthesis and Preparation

All reagents were obtained from commercial vendors and used without further purification. UHP-grade (99.999% purity) nitrogen and helium were used for all adsorption measurements. Powder X-ray diffraction patterns were collected on a Bruker D8 Advance diffractometer with a Cu anode (λ= 1.5406 Å).

Preparation of Na-faujasite, Na-mordenite, and Ni-Na-X zeolites

Na-faujasite (Si:Al = 2.6) and Na-mordenite (Si:Al = 6.5) were purchased from Zeolyst. Na-faujasite samples were dried at 413 K under vacuum to remove residual adsorbed water. Due to smaller pore sizes and evidence of residual water after the previous vacuum drying, Na-mordenite samples were treated with a more rigorous calcination procedure as reported in literature.[1] N_2 adsorption experiments were carried out on the dried samples using a Micromeritics Tristar 3000 instrument.

To investigate the effect of paramagnetic ions on the relaxation behavior of Na-faujasite, Ni–Na-X was prepared and characterized as previously reported.[1]

Synthesis and activation of Mg_2(dobdc)

The compound Mg_2(dobdc) was prepared and activated according to literature procedure.[2] The successful synthesis and activation of the framework was confirmed by comparing the X-ray powder diffraction pattern and Langmuir and BET surface areas to those previously reported (see Figure S1).

Synthesis and activation of Zn_2(dobdc)

The compound Zn_2(dobdc) was synthesized and activated in a manner similar to that previously reported.[2a] Here, $Zn(NO_3)_2$•$6H_2O$ (1.911 g, 6.424 mmol) and 2,5-dihydroxyterephthalic acid (H_4dobdc) (0.5760 g, 2.907 mmol) were dissolved in a mixture of 240 mL of N,N, dimethylformamide (DMF), 16 mL of absolute ethanol, and 16 mL of deionized water. This solution was distributed into twenty-four 20 mL vials and heated on a dry bath at 120 °C for 24 hours. The yellow microcrystalline Zn_2(dobdc) was collected from the vials and combined into a 100 mL jar. The mother liquor was exchanged for anhydrous DMF, and the sample was transferred to a glove box. The material was soaked in DMF at 100 °C. The DMF was exchanged four times over a period of two days. Similarly, methanol washes at 70 °C were performed every 8 hours for a total of eight washes. The material was then activated under vacuum for 24 hours at 180 °C prior to the 77 K N_2 adsorption measurement. The successful synthesis and activation of the framework was confirmed by comparing the X-ray powder diffraction pattern and Langmuir and BET surface areas to those previously reported (see Figure S2).

Synthesis and activation of Co_2(dobdc)

Co_2(dobdc) was prepared and activated according to literature procedure.[2a] Here, the red microcrystalline Co_2(dobdc) was activated under vacuum for 24 hours at 180 °C after DMF and methanol washes. The successful synthesis and activation of the framework was confirmed by comparing the X-ray powder diffraction pattern and Langmuir and BET surface areas to those previously reported (see Figure S3).

Synthesis and activation of Ni_2(dobdc)

Ni_2(dobdc) was prepared and activated according to literature procedure.[2a] Here, the brown microcrystalline Ni_2(dobdc) was activated under vacuum for 24 hours at 180 °C after DMF and methanol washes. The successful synthesis and activation of the framework was confirmed by comparing the X-ray powder diffraction pattern and Langmuir and BET surface areas to those previously reported (see Figure S4).

Synthesis and activation of Cu-HKUST-1

The compound Cu-HKUST-1 was synthesized and activated in a manner similar to that previously reported.[3] Here, $Cu(NO_3)_2$•$2.5H_2O$ (8.750 g, 37.63 mmol) and 1,3,5 benzene tricarboxylic acid (H_3BTC) (4.200 g, 20.00 mmol) were dissolved in 250 mL of absolute ethanol in a 500 mL round-bottom flask. The resulting solution was refluxed at 70 °C for 48 hours. The resulting blue Cu-HKUST-1 was recovered by filtration and placed under vacuum at 100°C for 24 hours until the material turned a deep purple. The successful synthesis and activation of the framework was confirmed by comparing the X-ray powder diffraction pattern and Langmuir and BET surface areas to those previously reported (see Figure S5).

Synthesis and activation of UiO-66

The compound UiO-66 was synthesized and activated in a manner similar to that previously reported.[4] Here, $ZrCl_4$ (0.4672 g, 2.000 mmol) and 1,4 benzene-dicarboxylic acid (H_2BDC) (0.6589 g, 4.000 mmol) were dissolved in 77 mL of DMF and 3.4 mL of acetic acid. This stock solution was distributed into eight 20 mL vials. The vials were heated on a dry bath at 120 °C for 24 hours. The resulting white powder was recovered by filtration. Four DMF exchanges were performed at 70 °C over the course of two days. The DMF was then decanted and replaced with CH_2Cl_2. The UiO-66 was soaked in CH_2Cl_2 at 25°C for a minimum of 6 hours between each of

the 6 CH_2Cl_2 exchanges. The UiO-66 was then activated under dynamic vacuum at 120 °C for 24 hours. The successful synthesis and activation of the framework was confirmed by comparing the X-ray powder diffraction pattern and Langmuir and BET surface areas to those previously reported (see Figure S6).

Gas Adsorption Measurements

Gas adsorption isotherms were measured using a Micromeritics ASAP 2020 instrument. Samples were transferred under a dinitrogen atmosphere to preweighed analysis tubes, which were capped with a Transeal. The samples were evacuated on the ASAP until the outgas rate was less than 2 mTorr/min. The evacuated analysis tubes containing degassed samples were then carefully transferred to an electronic balance and weighed to determine the mass of sample (typically 50 – 250 mg). The tube was transferred back to the analysis port of the gas adsorption instrument. The outgas rate was again confirmed to be less than 2 mTorr/min. Langmuir and BET surface areas were determined by measuring N_2 adsorption isotherms in a 77 K liquid nitrogen bath and calculated using the Micromeritics software.

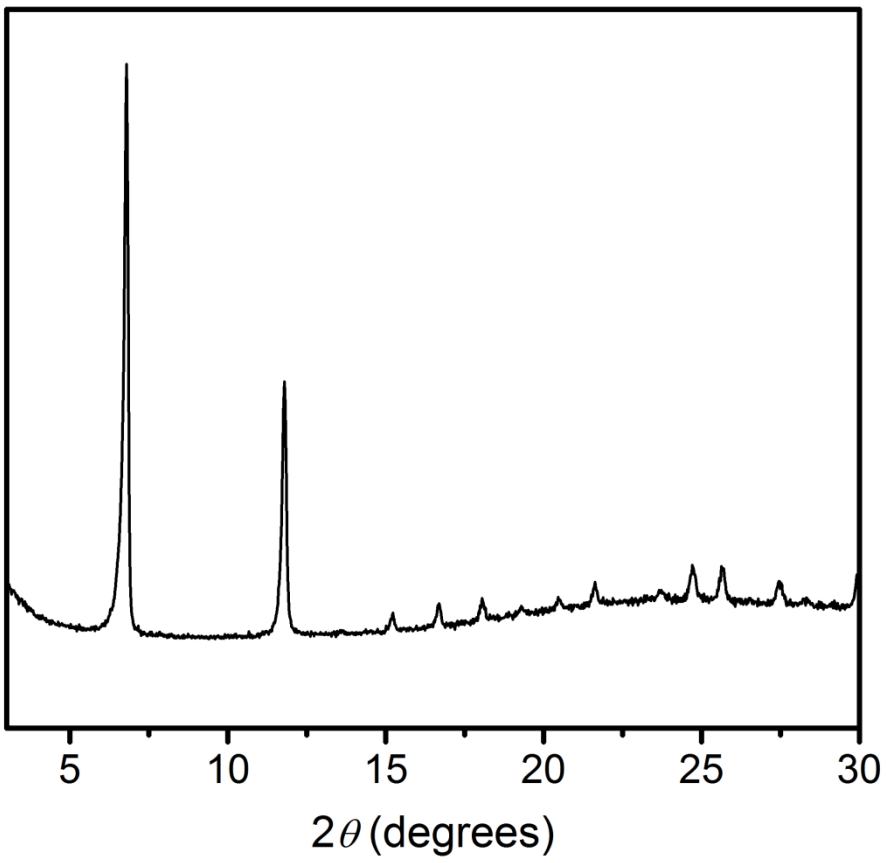

Figure S1. Powder X-ray diffraction pattern of as-synthesized Mg_2(dobdc).

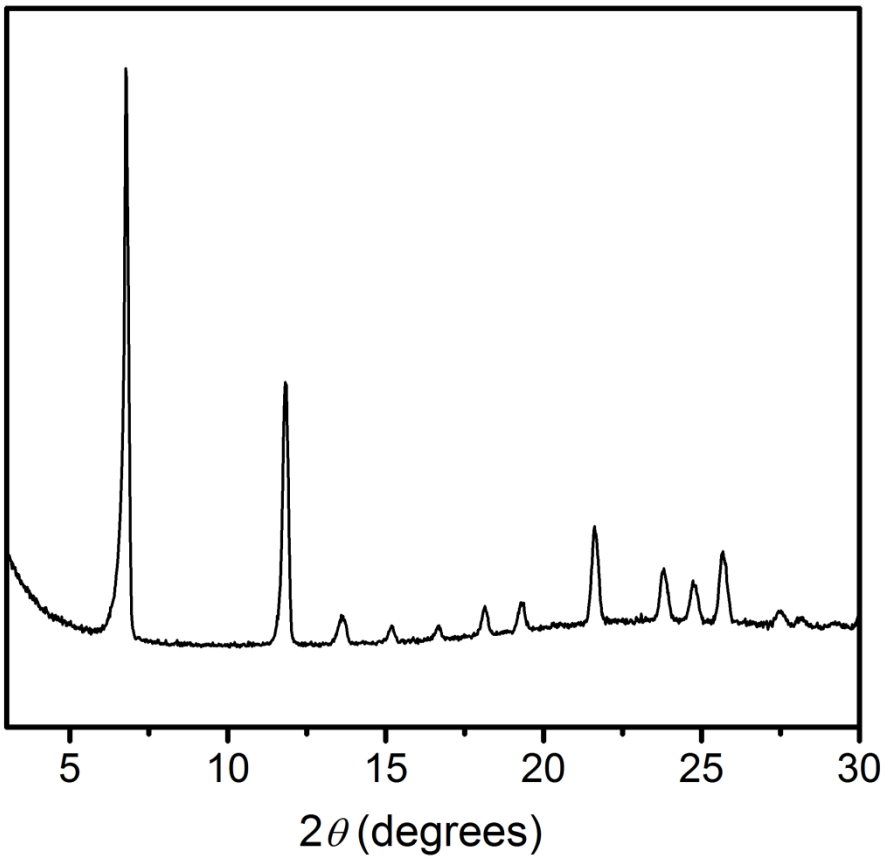

Figure S2. Powder X-ray diffraction pattern of as-synthesized Zn_2(dobdc).

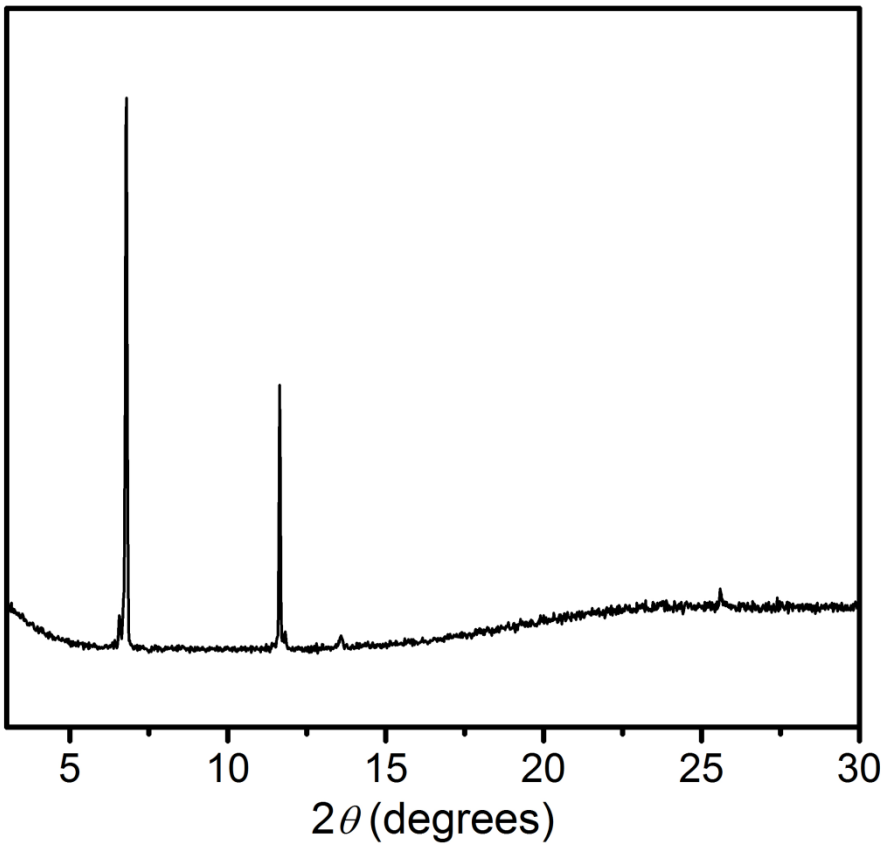

Figure S3. Powder X-ray diffraction pattern of as-synthesized Co_2(dobdc).

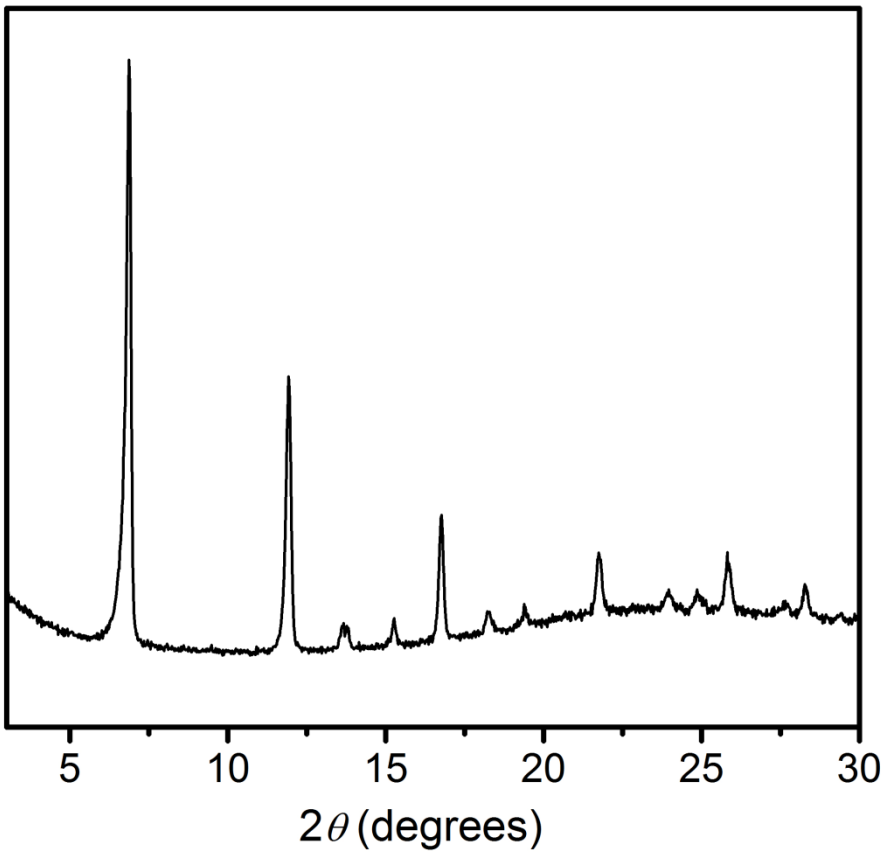

Figure S4. Powder X-ray diffraction pattern of as-synthesized Ni_2(dobdc).

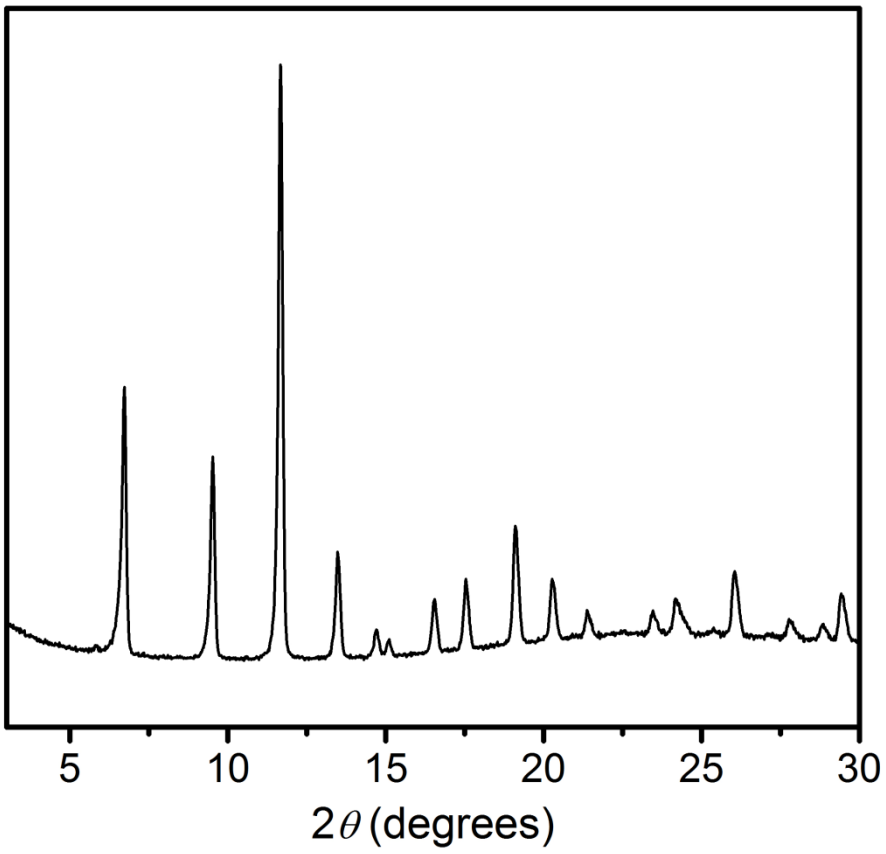

Figure S5. Powder X-ray diffraction pattern of as-synthesized Cu-HKUST-1.

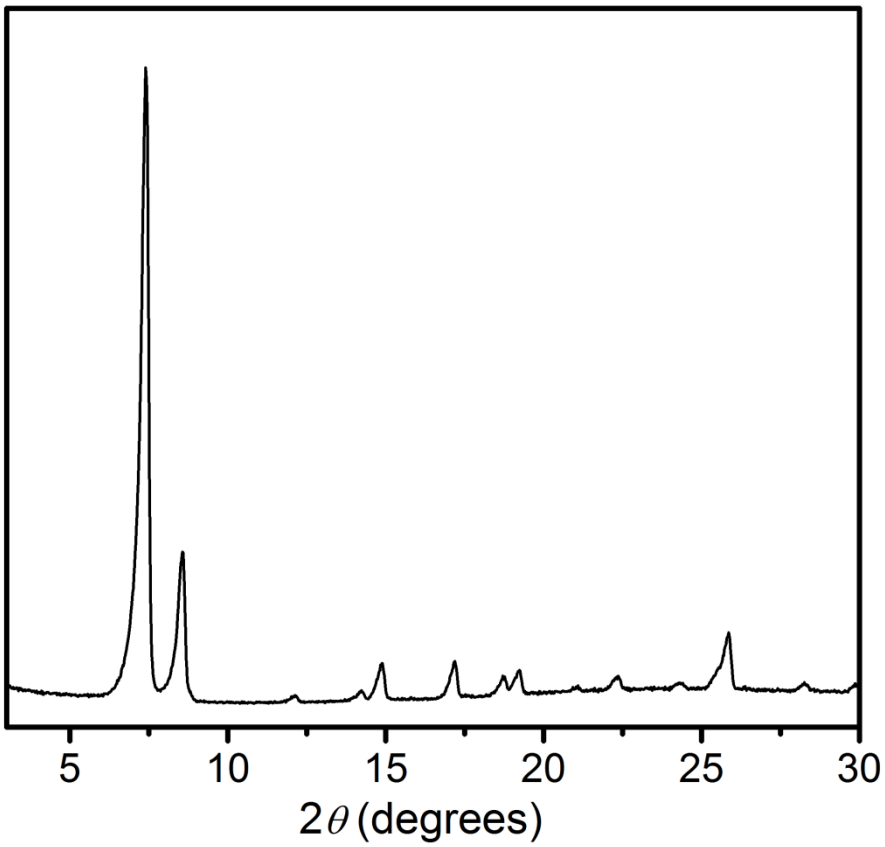

Figure S6. Powder X-ray diffraction pattern of as-synthesized UiO-66.

II. N_2 Adsorption Data

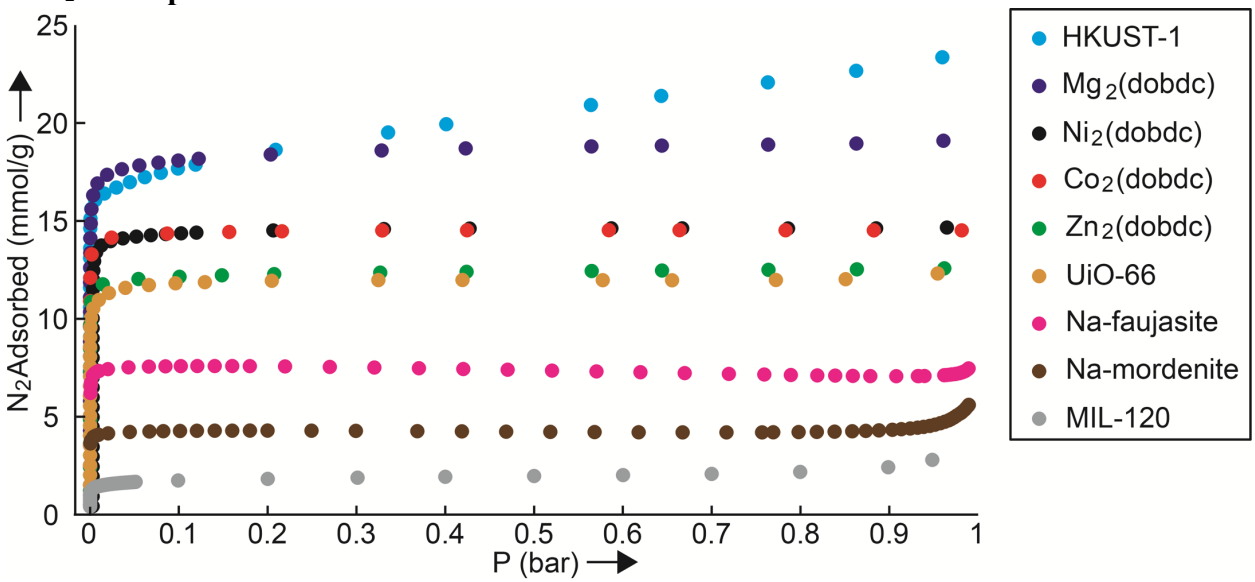

Figure S7. N_2 adsorption curves for all tested materials.

III. NMR Experimental Procedures

^{1}H-NMR relaxation was measured using a single-sided 13.1 MHz Profile NMR-MOUSE magnet[5] where the sample is placed in the stray field of a permanent magnet (Fig. S8) with a linear gradient of 7 T/m. A Kea II spectrometer was used for pulse generation and signal acquisition, and all pulse programs, including automation software, was written using Prospa v3.11 software package. An automated sample handler built by J-KEM Scientific was used to handle vials from a 96-vial holder, and interfaces with the Kea II spectrometer via TTL outputs. Custom software was provided with the sample handler. NMR experiments are synced with the autosampler by sending on/off signals from the spectrometer to the robot, which is then interpreted by the autosampler software as a command to add/remove sample vials.

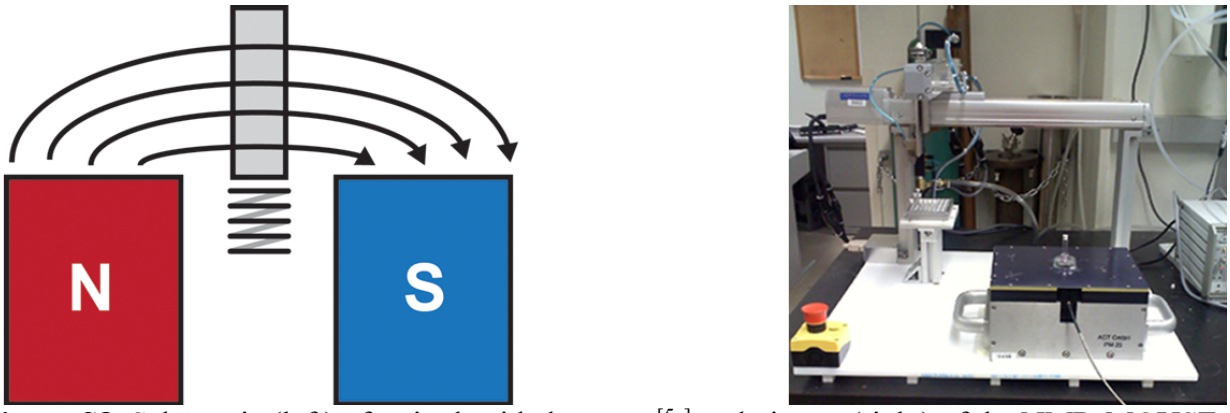

Figure S8. Schematic (left) of a single-sided magnet[5a] and picture (right) of the NMR-MOUSE with automation hardware

This geometry imposes fewer restrictions on sample geometry and also simplifies the incorporation of automation hardware. However, due to the strong static field gradients present in single-sided setups, Carr-Purcell-Meiboom-Gill (CPMG) pulse sequences[6] must be used to measure magnetization. Such pulse sequences include a series of refocusing RF pulses to counteract the effects of inhomogeneous fields. Furthermore, the field gradient imposes a large spread in Larmor frequencies across a macroscopic sample, and thus, RF pulses will only excite a small section of a given sample (~800 μm). The pulse sequence parameters were optimized for accurate detection of short T_2 components and for maximum signal (2 μs excitation pulses with an echo time of 55 μs).[7] A variable number of echoes were used, and the recycle delay was determined using saturation recovery experiments on each sample.

MOFs were imbibed by flashing the solvent into an evacuated (~7 Pa for one hour) chamber containing the MOF then allowing the MOF to soak overnight. This ensured that no gas would be trapped in the MOF so that the solvent would fully penetrate any accessible pore volume. The MOFs were then filtered and dried in a N_2 atmosphere to evaporate excess solvent. Subsequent thermogravimetric analysis (TGA Q50, TA Instruments, New Castle, DE) was used to quantify solvent content of the solvent-filled MOF. Approximately 3 mg of solvent-loaded powder was placed on a 100 μL platinum sample pan. Samples were held at room temperature for 10 minutes then heated to 500°C at 1°C/min under a nitrogen purge. Solvent content was determined from the mass loss prior to degradation temperatures for each material. Solvent

content was normalized to the dry weight of the MOF sample, and was systematically varied by micropipette addition or thermal evaporation. Finally, NMR experiments were conducted using the same MOF samples tested by adsorption experiments and focused on collecting NMR data with higher signal-to-noise, though the measurement time was still kept to a reasonable length in light of high-throughput requirements (~30 minutes per CPMG experiment). Identical NMR experiments were performed multiple times on each sample to quantify the error of the NMR experiment as well as the variability of the least-squares fit to experimental noise. Each sample consisted of ~10-15 mg of solvent-loaded MOF in a 6 mm ID glass vial tightly sealed with a plastic cap.

The effect of the static field gradient on the relaxation behavior of solvent-filled samples was tested by comparing relaxation data obtained on the NMR-MOUSE to that obtained from a 13 MHz homogeneous field permanent magnet. The relaxation time for the pore-confined solvent remained unchanged, though the inter-particle solvent T_2 was lengthened significantly (the T_2 for neat DMSO in a homogeneous field is ~2s compared to ~300ms on the NMR-MOUSE). Because the analysis detailed in this study only requires that the pore-confined and inter-particle T_2's be distinguishable, the effects of the field gradient can be disregarded.

However, the field gradient of the NMR-MOUSE does significantly decrease the obtainable signal to noise ratio (SNR) due to slice selection. To increase the SNR and decrease the measurement time, a small permanent magnet, such as a Halbach array, could be used in conjunction with a standard volume solenoid coil without loss of automation functionality. The experiments conducted on the 13 MHz homogeneous field permanent magnet described above reduced the experiment time an order of magnitude to a few minutes per sample. Individual samples of frameworks at different solvent contents can be provided by the existing high-throughput hardware, and thus, solvent-content modulation should not be a limiting factor for throughput. In comparison, BET experiments can take 24 hours or more depending on the porosity of the framework, as equilibriation can take a considerable time within the low-pressure region of the adsorption isotherm. Substantial time savings are also gained by simplifying sample preparation. The sample preparation for BET measurements, which includes isolation, washing and complete evacuation of the solid, can take up to a week depending on the sample (especially samples that require solvent exchange and open metal sites). Finally, the NMR technique only requires simple liquids-handling automation hardware, benefitting in cost and ease of operation over a potential high-throughput gas adsorption setup.

IV. NMR Data Analysis Procedures

An algorithm for finding numerical solutions to a Fredholm integral equation of the first kind, known colloquially as an inverse Laplace transform (ILT),[8] deconvolutes multi-exponential transverse relaxation into individual components. The ILT seeks to minimize the mismatch between the acquired data and the summation of prescribed exponential components.

$$S_n(t) = \sum_k C_k e^{-t_n/T_k} + \varepsilon_n \qquad \text{(S1)}$$

$$min\left[\sum_{n=1}^{N}\left(S_n(t)-\sum_{j=1}^{M}C_j e^{-t_n/T_j}\right)^2+\alpha^{-2}f''\right] \quad \text{(S2)}$$

Eq. S1 describes S_n, the acquired NMR signal at time t_n composed of various exponential components with relaxation times T_k and weights C_k, added to any experimental noise ε. In Eq. S2, for N time points, the data are fitted with M exponential components with relaxation times T_j and weights C_j to minimize the least-squares error χ^2, generating a spectrum of relaxation components. Due to experimental error and the number of fitting parameters, this least-squares minimization is ill-posed. Regularization constrains the set of possible solutions such that the solution must be smooth.[9] An additional constraint *f''*, a numerical estimation for the second derivative of the solution spectrum, is added and weighted by the smoothing parameter α. Thus, minimization of the magnitude of the second derivative produces smoothly-varying spectra. The parameter α exhibits a large effect on the resulting exponential spectra and is chosen by a process called the L-curve which balances the degree of smoothing with the squared error. In general, overly small values of α enforce the smoothing constraint at the expense of fitting the data, while overly large values of α fit the data too closely, increasing the effect of noise. Thus, the proper selection of α extracts maximum information while rejecting the effects of experimental noise. Lower signal-to-noise necessitates smaller α (greater smoothing), coarsening the spectra and limiting the resolution of different relaxation populations. Effects of experimental noise on the resolution of the ILT (ΔT_{ILT}) can be approximated by Eq. S3, where the resolution is defined as the ratio of the two relaxation times to be distinguished.

$$\log(\Delta T_{ILT}) = \frac{\log(T_{max}/T_{min})}{1.2\ln(M(0)/\sigma)} \quad \text{(S3)}$$

Here, M(0) is the initial or maximum signal intensity, σ is the standard deviation of the noise, and $T_{max/min}$ represent the limits of the chosen time constants for the ILT.[10]

The Laplace inversion was applied to CPMG relaxation decays with a logarithmically-spaced range of relaxation times (0.01 ms – 1000 ms) relevant for the NMR-MOUSE. The smoothing parameter was chosen automatically by calculating the maximum of the second derivative of the L-curve and taking the α value corresponding to that maximum. In the event that the L-curve fails and no maximum is found, the data are not used. Also, the Laplace inversion may give artifacts, defined as non-zero value at the endpoints of the distribution, independent of the choice of minimum and maximum relaxation times. These artifacts indicate a poor fit to the data, and any data yielding artifacts at short relaxation times were discarded, as this is the region of interest. Data with long relaxation time artifacts were generally correctable by omitting a small number of data points at the end of each decay. The code for this data analysis was programmed into MATLAB.

To extract the pore volume from the Laplace inversion, the peaks were integrated, and the fraction of total intensity of the peak with the shortest T_2 (x_{pore}) was calculated. This peak was associated with the pore-confined solvent (S_{pore}) However, due to small amounts of strongly-bound, immobile solvent with very short T_2 (~10 μs) that go undetected, the signal intensities do not directly correspond to solvent volume. The following correction was applied to account for this effect.

$$S_{pore} \propto V_{pore} - V_{im} \quad \text{(S4)}$$

$$S_{total} \propto V_{total} - V_{im} \quad \text{(S5)}$$

In the above expressions, V_{pore} and V_{bulk} represent the true pore volume and total volume respectively; V_{im} represents the volume of immobile, undetected solvent; S_{total} represents the total intensity; and $x_{pore} = S_{pore}/S_{total}$. Substitution of Eq. S4 and S5 for x_{pore} leads to Eq. 1 in the main text.

V. Selected TGA Data

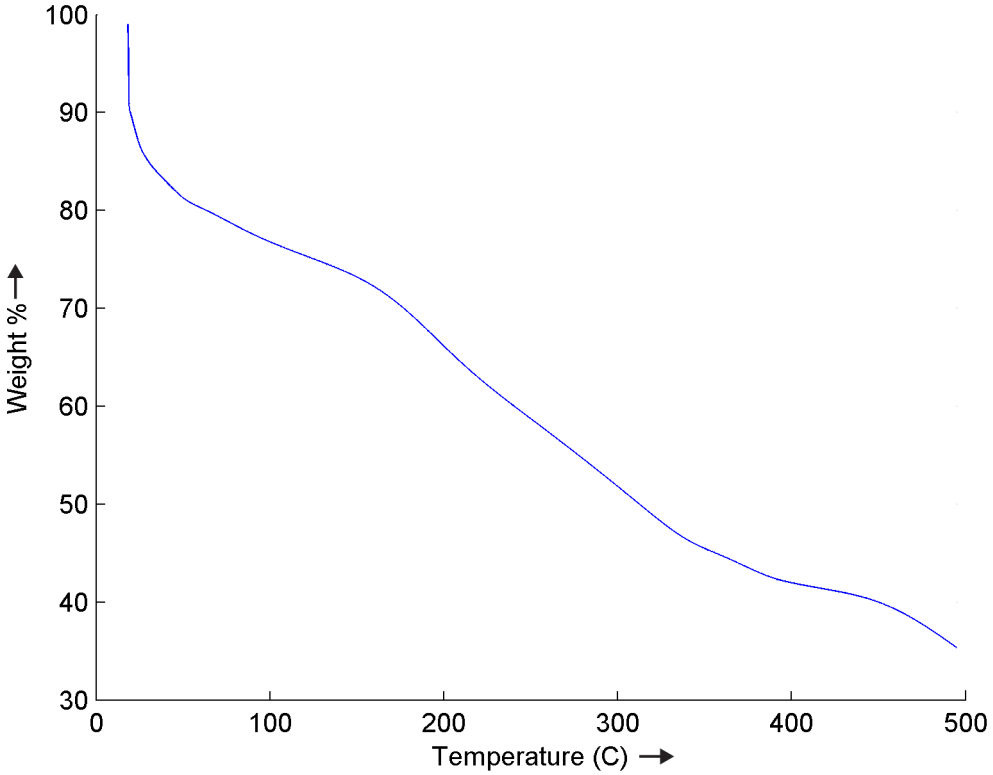

Figure S9. TGA curve of Mg_2(dobdc) loaded with DMF

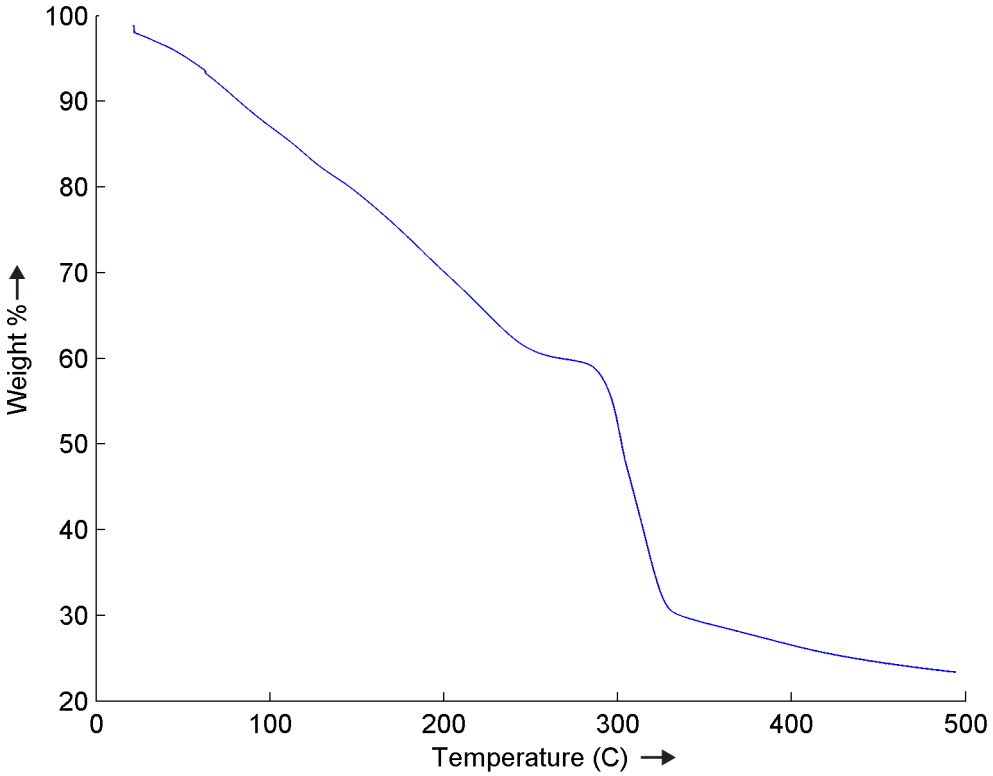

Figure S10. TGA curve of HKUST-1 loaded with DMF

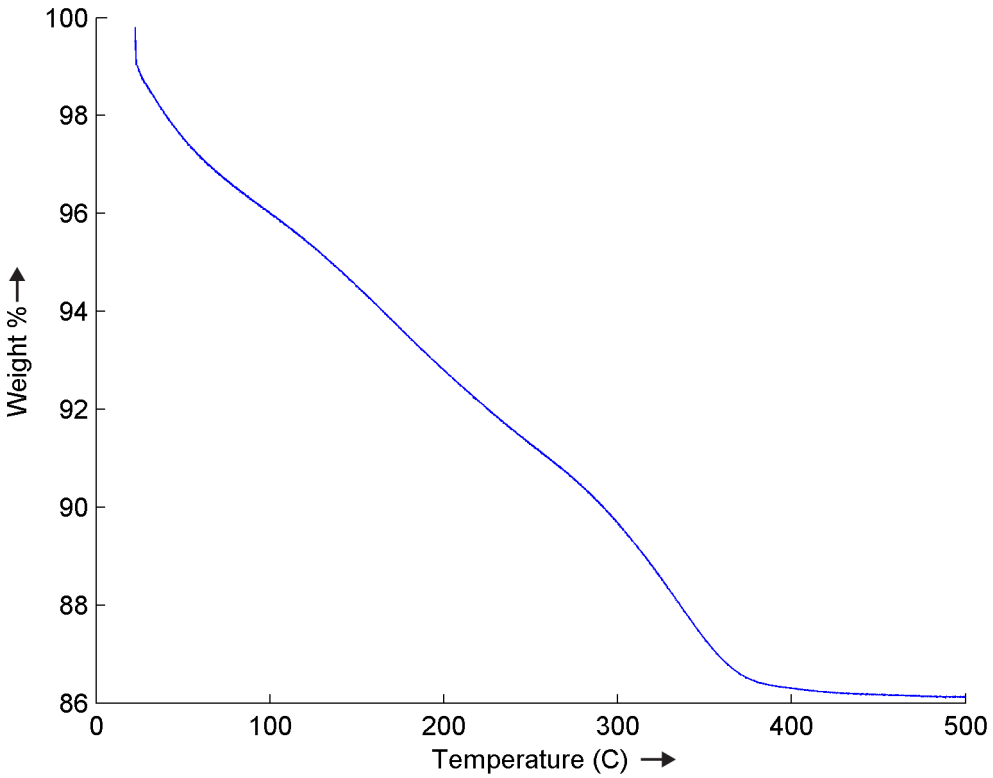

Figure S11. TGA curve of Na-mordenite loaded with DMF

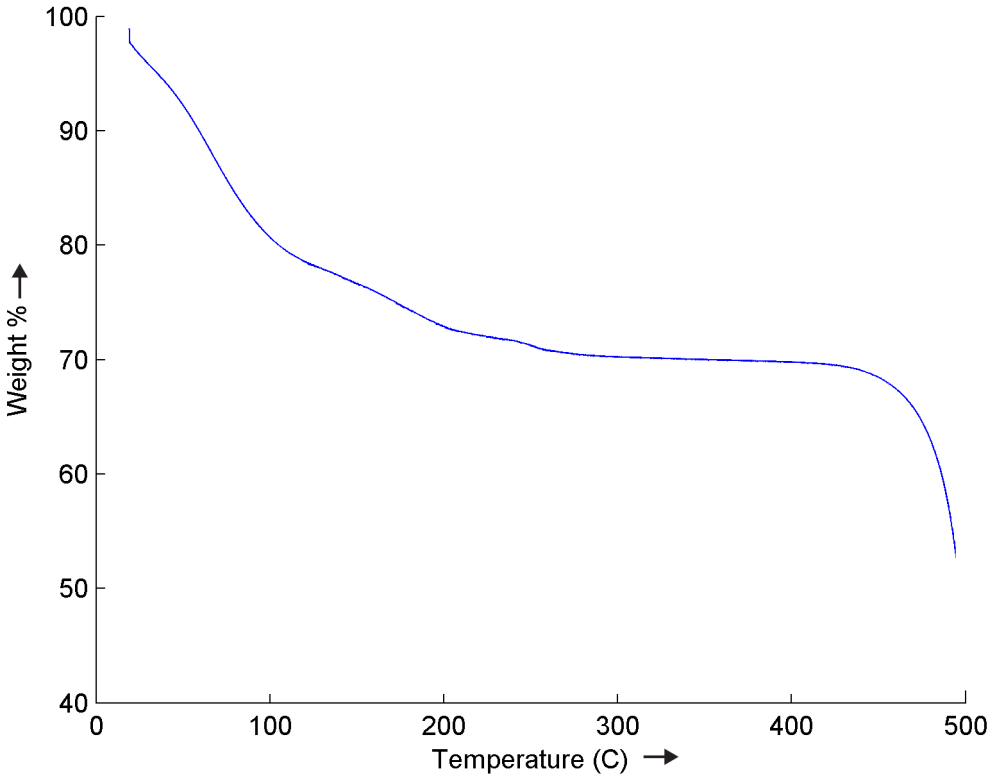

Figure S12. TGA curve of UIO-66 loaded with DMF

VI. Selected NMR Relaxation Data

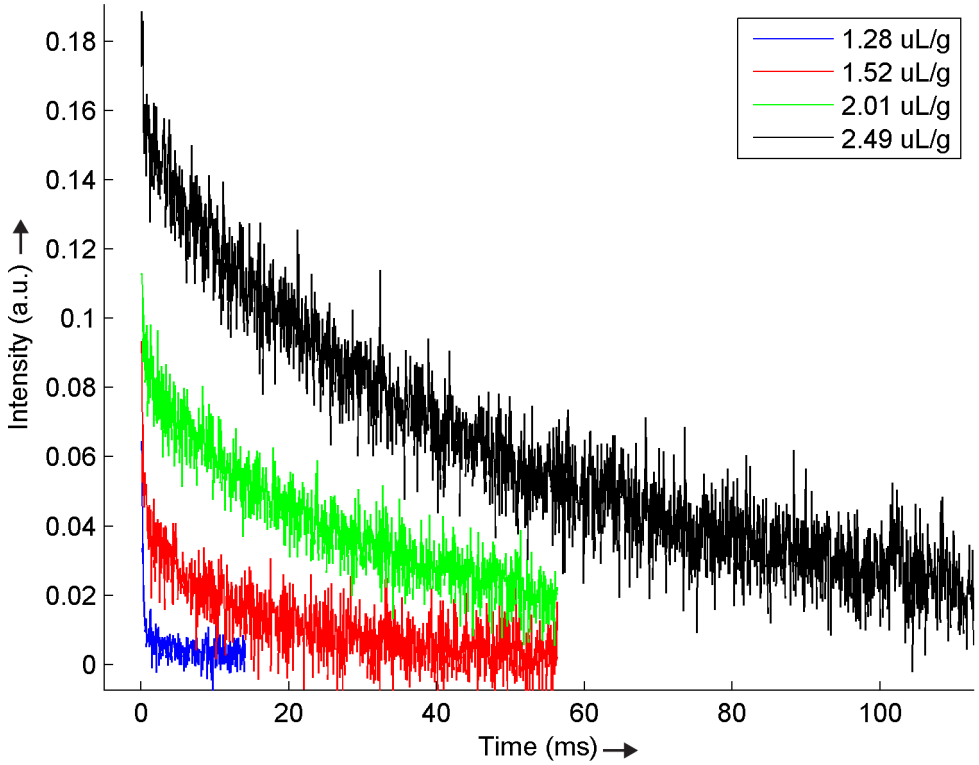

Figure S13. Raw relaxation data of Mg_2(dobdc) loaded with DMF

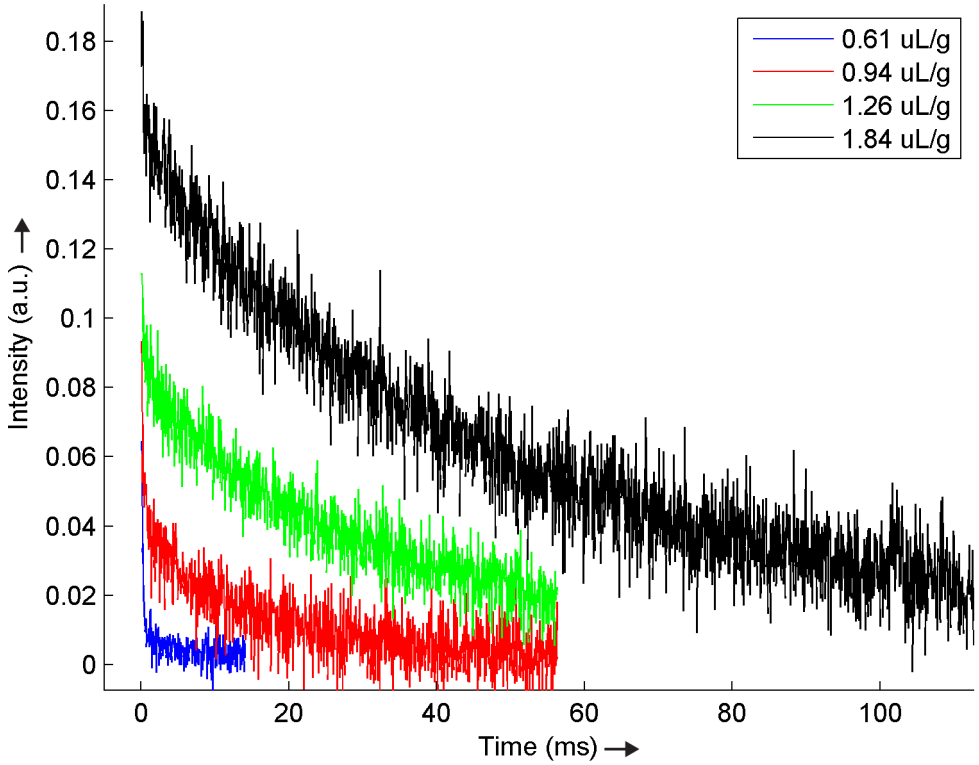

Figure S14. Raw relaxation data of HKUST-1 loaded with DMF

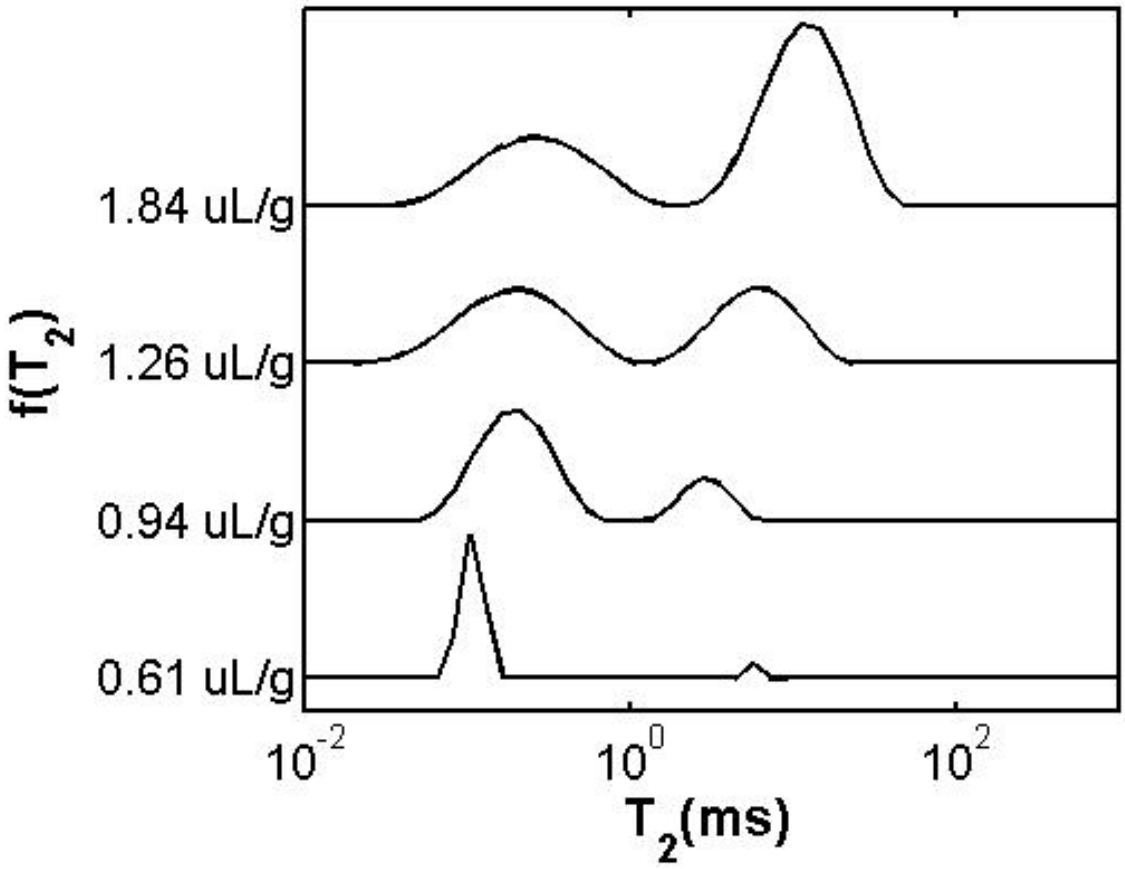

Figure S15. Relaxation spectra of HKUST-1 loaded with DMF obtained from Laplace inversion

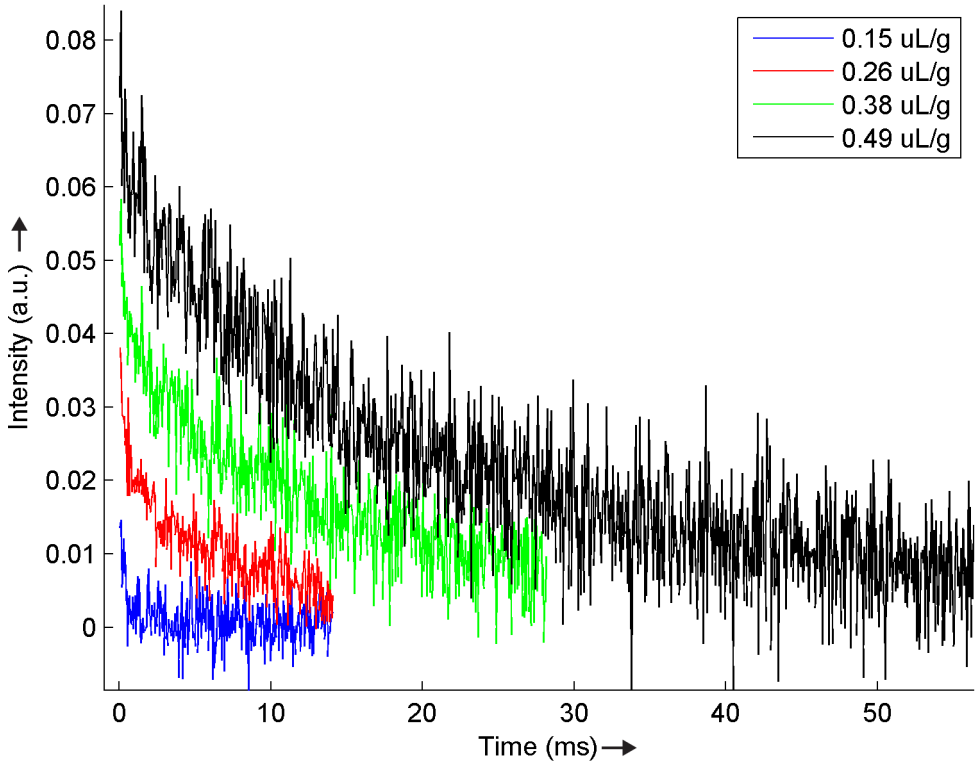

Figure S16. Raw relaxation data of Na-mordenite loaded with DMF

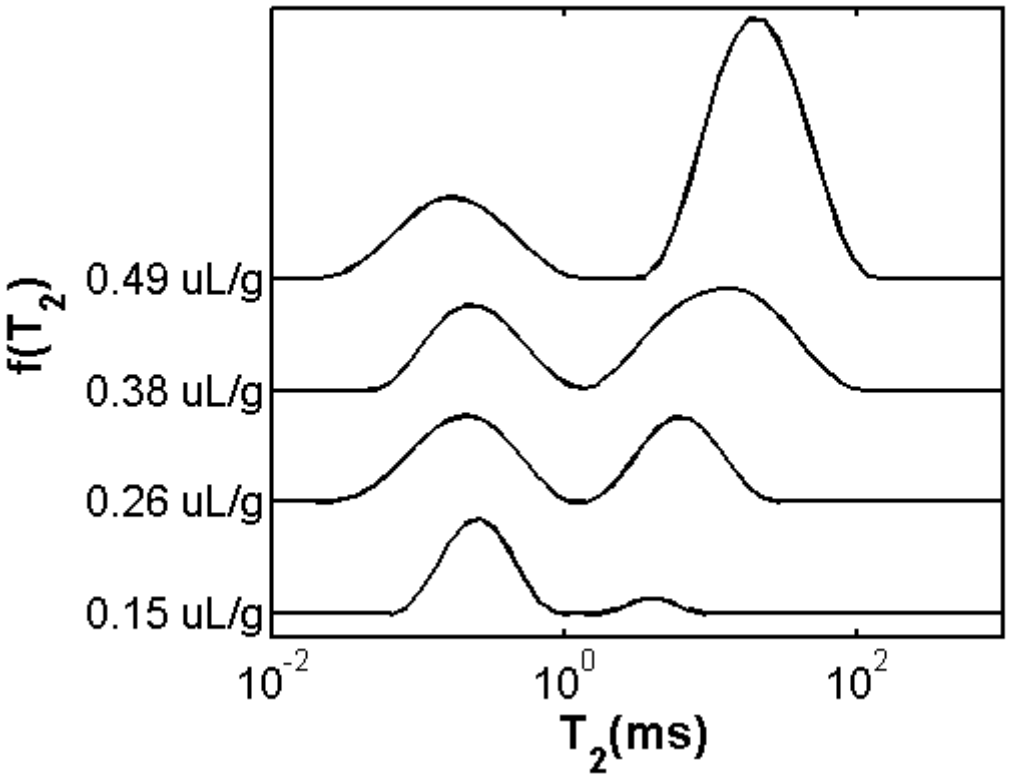

Figure S17. Relaxation spectra of Na-mordenite loaded with DMF obtained from Laplace inversion

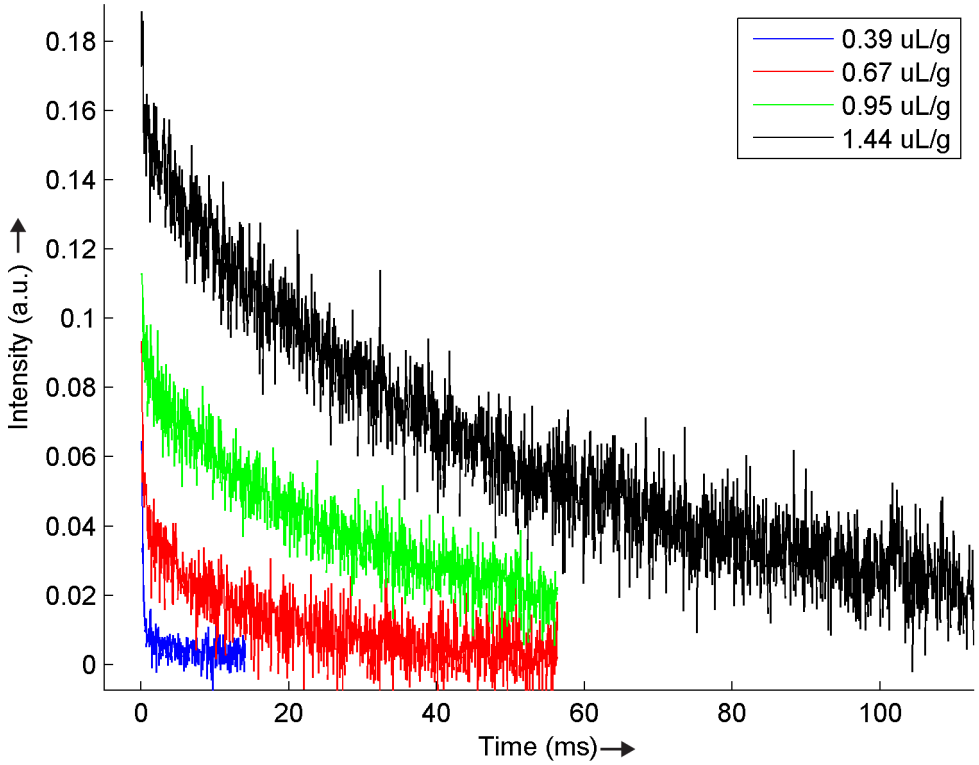

Figure S18. Raw relaxation data of UiO-66 loaded with DMF

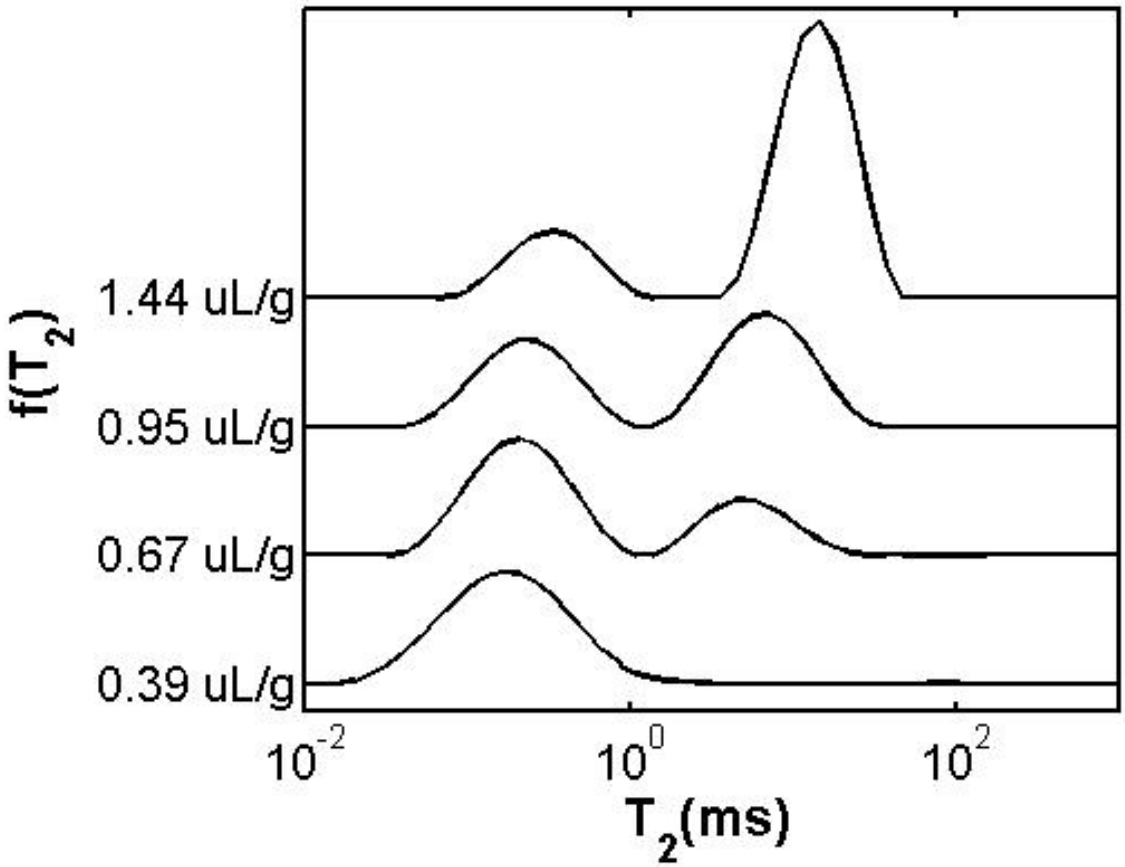

Figure S19. Relaxation spectra of UiO-66 loaded with DMF obtained from Laplace inversion

VII. Predicted NMR Surface Areas

Table S1. Predicted surface area from NMR relaxation-BET surface area correlation

Sample name	BET surface area (m^2/g)	NMR-DMSO surface area (m^2/g)	NMR-DMSO surface area % error	NMR-DMF surface area (m^2/g)	NMR-DMF surface area % error
Mg_2(dobdc)	1662	1780 ± 166	+7	1921 ± 152	+16
Zn_2(dobdc)	1133	1297 ± 163	+14	1066 ± 149	-6
Co_2(dobdc)	1347	1240 ± 164	-8	1180 ± 152	-12
Ni_2(dobdc)	1341	962 ± 180	-28	1306 ± 151	-3
HKUST-1	1583	1391 ± 163	-12	1305 ± 150	-18
UiO-66	1084	1132 ± 163	+4	1000 ± 149	-8
Ni-NaX zeolite	774	806 ± 163	+4	814 ± 151	+5
Na-faujasite	714	946 ± 163	+33	845 ± 151	+18
Na-mordenite	398	481 ± 166	+21	600 ± 150	+50

VIII. Bloch-Torrey Model

A PDE model was developed to further elucidate the physics of a diffusing, heterogeneous MOF-solvent system. This model utilizes the Bloch-Torrey equations to describe the evolution of NMR magnetization in a single spherically-symmetric particle of radius R_1 surrounded by varying amounts of bulk solvent of thickness R_2 (see Figure S20 below).

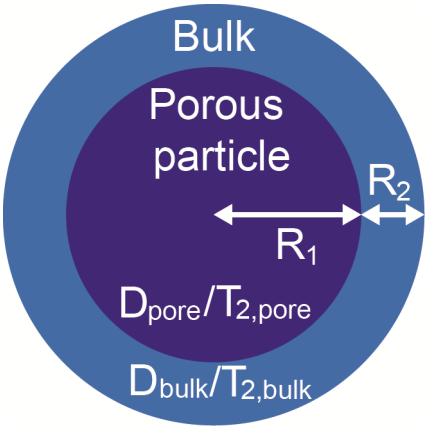

Figure S20. Particle-film model describing relaxation of solvent on MOFs.

The resulting conservation equation (Eq. S6), boundary conditions (Eq. S7-9), and initial condition (Eq. S10) are shown below.

$$\frac{\partial M}{\partial t} = \frac{D_{bulk/pore}}{r^2}\frac{\partial}{\partial r}\left(r^2 M\right) - \frac{M}{T_{2,bulk/pore}} \quad \text{(S6)}$$

$$0 = \left.\frac{\partial M}{\partial r}\right|_{r=0} \quad M|_{r=0} < \infty \quad \text{(S7, S8)}$$

$$0 = \left[M|_{r=R_1-} - M|_{r=R_1+}\right] = \left[\left(D_{pore}\frac{\partial M}{\partial r}\right)\Big|_{r=R_1-} - \left(D_{bulk}\frac{\partial M}{\partial r}\right)\Big|_{r=R_1+}\right] \quad \text{(S9)}$$

$$M(t=0) = M_0 \quad \text{(S10)}$$

In the above equations, M represents the density of magnetization, D represents the solvent diffusion coefficient inside the particle or in the bulk film, and T_2 represents the volumetric relaxation time of either the particle or the bulk film. In general, $D_{pore} < D_{bulk}$ and $T_{2,\,pore} < T_{2,\,bulk}$ due to restriction by and interactions with the pore walls. The model provides for the temporal decay of the NMR signal due to relaxation and diffusion. Note that the solvent relaxation inside the particle, modeled as a bulk reaction, is assumed to be homogeneous, as the diffusion length of a solvent molecule is typically larger than the pore diameter of MOFs.

Parameters used for Figure 4 in the main text are R_1 = 10 µm, R_2 = 10 µm, $T_{2,\,pore}$ = 1 ms, $T_{2,\,bulk}$ = 300 ms, and $D_{pore} = D_{bulk} = 7 \times 10^{-10}$ m^2/s. Note that the diffusion coefficient inside the porous media is set to be equal to the bulk diffusion coefficient (measured from neat DMSO). Though diffusion in porous media is generally restricted, this limiting case helps illustrate the source of intermediate relaxation peaks. Also, the relaxation values are set at values typically found when testing porous materials on the NMR-MOUSE, and the interface is arbitrarily defined as the region spanned by [R_1,R_1+5 µm].

[1] A. N. Mlinar, G. B. Baur, G. G. Bong, A. Getsoian, A. T. Bell, *J. Catal.* **2012**.
[2] a) S. R. Caskey, A. G. Wong-Foy, A. J. Matzger, *J. Am. Chem. Soc.* **2008**, *130*, 10870-10871; b) K. Sumida, C. M. Brown, Z. R. Herm, S. Chavan, S. Bordiga, J. R. Long, *Chem. Commun. (Cambridge, U. K.)* **2011**, *47*, 1157-1159.
[3] S. S. Chui, *Science* **1999**, *283*, 1148-1150.
[4] a) J. H. Cavka, S. Jakobsen, U. Olsbye, N. Guillou, C. Lamberti, S. Bordiga, K. P. Lillerud, *J. Am. Chem. Soc.* **2008**, *130*, 13850-13851; b) A. Schaate, P. Roy, A. Godt, J. Lippke, F. Waltz, M. Wiebcke, P. Behrens, *Chemistry* **2011**, *17*, 6643-6651.
[5] a) B. Blümich, J. Perlo, F. Casanova, *Prog. Nucl. Magn. Reson. Spectrosc.* **2008**, *52*, 197-269; b) G. Eidmann, R. Savelsberg, P. Blümler, B. Blümich, *J. Magn. Reson.* **1996**, *122*, 104-109; c) J. Perlo, F. Casanova, B. Blumich, *J. Magn. Reson.* **2005**, *176*, 64-70.
[6] a) H. Carr, E. Purcell, *Physical Review* **1954**, *94*, 630-638; b) S. Meiboom, D. Gill, *Rev. Sci. Instrum.* **1958**, *29*, 688-691.
[7] F. Casanova, J. Perlo, B. Blümich, *Single-sided NMR*, Springer, **2011**.
[8] a) S. W. Provencher, *Comput. Phys. Commun.* **1982**, *27*, 213-227; b) L. Venkataramanan, Y. Q. Song, M. D. Hurlimann, *IEEE T. Signal Proces.* **2002**, *50*, 1017-1026.
[9] a) G. Borgia, R. Brown, P. Fantazzini, *J. Magn. Reson.* **1998**, *132*, 65-77; b) P. C. Hansen, *SIAM Rev.* **1992**, *34*, 561-580.
[10] Y. Q. Song, L. Venkataramanan, L. Burcaw, *J. Chem. Phys.* **2005**, *122*, 104104.